Chemical composition tuning in quaternary *p*-type Pb-chalcogenides - A promising strategy for enhanced thermoelectric performance

Sima Aminorroaya Yamini,*[a] Heng Wang[b] , Zachary M. Gibbs[c], Yanzhong Pei[d], Shi Xue Dou[a], and G Jeffrey Snyder *[b]

[a] Australian Institute for Innovative Materials (AIIM), Innovation Campus, University of Wollongong, NSW 2519, Australia.
Fax: +61242215731; Tel: +61242981401; E-mail: sima@uow.edu.au

[b] Materials Science, California Institute of Technology, Pasadena, CA 91125, USA.
Tel: +16265026126; E-mail: jsnyder@caltech.edu

[c] Department of Chemistry and Chemical Engineering, California Institute of Technology, Pasadena, CA 91125, USA.

[d] School of Materials Science and Engineering, Tongji University, 4800 Caoan Road, Shanghai 201804, China.

Experimental

Resistivity and Hall measurements: High temperature Hall effect measurements were carried out with an in-house Hall apparatus. Samples were loaded onto a heated BN substrate, and four probes were attached to the edge of the sample. The sample was placed in vacuum with a magnetic field (up to ± 2 T) perpendicular to its surface. The resistivity (ρ) and Hall coefficient (R_H) along the hot pressing direction was measured using the van de Pauw method [1]. The typical size of samples for the high temperature measurement was 12 mm in diameter and ~1.5 mm in thickness. The experiments were performed from room temperature up to 850 K under vacuum. The carriers mobility ($\mu = R_H/\rho$) was then calculated based on the measured R_H.

Electron Microscopy Analyses: Scanning electron microscopy was performed on finely polished samples using a JEOL JSM-7500FA field emission gun-scanning electron microscope (FEG-SEM) equipped with a Bruker X-Flash 4010 energy dispersive spectroscopy (EDS) detector. Samples were characterized using a JEOL 2010 transmission electron microscope (TEM). TEM samples were prepared by cutting them into 3 mm diameter discs using a Leica TXP polisher, then grinding and polishing them to less than 100 μm in thickness, then dimpled which was followed by Ar-ion milling on a stage cooled with liquid nitrogen. During ion milling low voltages and currents were used to reduce damage on the samples.

Sodium solubility and precipitation

The XRD patterns of samples with $x < 0.1$ in Figure 1 appear to be single phase, whereas samples with $x > 0.1$ reveal two distinct phases. The complementary electron microscopy study was performed to confirm the single phases. The microstructure of samples $Pb_{0.98}Na_{0.02}S_xSe_{0.1}Te_{(0.9-x)}$, ($x$ = 0, 0.05 and 0.1) were studied by the field emission gun

scanning electron microscope (FEG-SEM). The cast samples and those were hand-ground, sintered and had been through several cycles of heating up to 850 K and cooling during transport properties measurements, were finely polished. SEM analysis revealed no trace of precipitates in samples with x = 0 and 0.05. The transmission electron microscope (TEM) analysis was performed on sintered sample with x = 0.05 to investigate the presence of nanoprecipitates. The TEM micrographs in Figure S1 clearly show the grain boundaries and single phase compound, free of nano-precipitates.

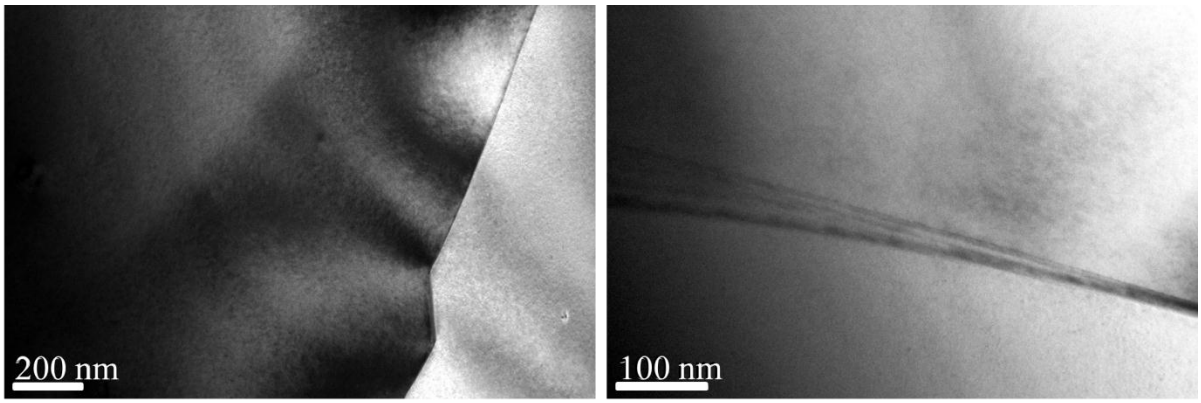

Figure S1: TEM micrograph of the $Pb_{0.98}Na_{0.02}S_{0.05}Se_{0.1}Te_{0.85}$ (S5), showing the grain boundaries and single phase compound free of nanoprecipitates. The sample has been through several cycles of heating up to 850 K and cooling during transport properties measurements.

A recent transmission electron microscopy study [2] on sodium-doped lead chalcogenides has concluded that the solubility limit of sodium in PbS (~ 2 at%) is higher than in PbSe (~ 0.9 at%) and much higher than PbTe (~ 0.5 at%). Moreover, our recent report on the solubility of sodium in PbTe at various temperature has shown the maximum solubility of sodium in PbTe ~0.7 at%.[3]. Samples from the current study were doped with 1 at% Na. The achieved single phase alloys demonstrates that the simultaneous alloying of PbTe by PbSe and PbS with higher sodium solubility limit has increased the solubility of sodium in the single phase $Pb_{0.98}Na_{0.02}S_{0.05}Se_{0.1}Te_{0.85}$ compound to more than 1 at%.

Although the scanning electron microscope (SEM) analysis of the cast sample $Pb_{0.98}Na_{0.02}S_{0.1}Se_{0.1}Te_{0.8}$ (S10) presented a single phase, the SEM micrograph of the sintered samples revealed in Figure S2 illustrates the presence of precipitates at grain boundaries. Elemental analysis obtained from precipitates using energy dispersive X-ray spectroscopy (EDS) detected high concentration of sulphur in the EDS, indicating sulphide precipitates within the matrix. The sintered sample was exposed to more than ten heating/cooling cycles in the transport properties measurements. This result indicates that sulphide precipitates probably exist in the cast sample at concentrations lower than XRD detection limit and in sizes smaller than SEM resolution. However, during electronic transport properties measurements of sintered samples at elevated temperature, sulphide precipitates dissolve in the matrix and reprecipitate upon cooling, preferentially at grain boundaries due to higher surface free energy. Sulphide precipitates at grain boundaries were detected by SEM in samples that had been through numerous heating/cooling cycles. Therefore, we believe that the maximum solubility of PbS in $PbSe_{0.1}Te_{0.9}$ is less than 10 at% and more than 5 at%.

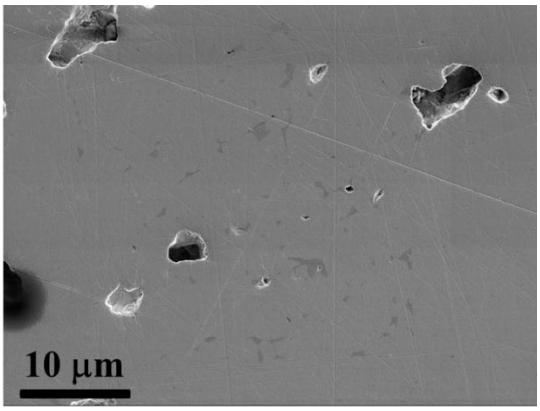

Figure S2: SEM micrograph of the sintered sample $Pb_{0.98}Na_{0.02}S_{0.1}Se_{0.1}Te_{0.8}$ (S10), showing the sulphide precipitates at grain boundaries. The sample has been through more than ten cycles of heating up to 850 K and cooling during transport properties measurements.

Electronic transport properties

The resistivity (ρ) and Hall coefficient, R_H, were measured for all samples over a heating and cooling cycle, using the van der Pauw method [1]. The resistivity values for heating and cooling are overlapped for single phase samples of $Pb_{0.98}Na_{0.02}S_xSe_{0.1}Te_{(1-x)}$ (x = 0, 0.05) as shown in Figure S3(a) and demonstrate a hysteresis for the sample with x = 0.1 which contains secondary phase of sulphide. The electrical resistivity exhibits a peak at approximately 600 K during heating that can be correlated to a deviation from an smoothly declining curve for Hall coefficient shown in Figure S3(b). The cycle was repeated several times, and various heating rates were employed to confirm the presence of hysteresis in resistivity for the composite sample. The measured hysteresis was similar and repeatable.

The Hall coefficient value depends on the carrier concentration, energy band structure, carrier scattering mechanism, and degree of degeneracy [4]. A similar carrier scattering mechanism and degree of degeneracy can be assumed for both the composite and the single phase samples. Therefore, the observed deviation in the Hall coefficient of the composite samples might originate from variations in carrier concentration and/or energy of the band structure within the samples.

The solubility of the secondary phase in the matrix of the pseudo-binary PbTe-PbS system increases at elevated temperature, as presented in the phase diagram [5]. Therefore, during electronic transport properties measurements at elevated temperatures, sulphur-rich precipitates in the composite sample are dissolved in the matrix and reprecipitate upon cooling. The dissolution of precipitates at elevated temperature could vary the energy of the band structure. The diffusion of atoms in solids is thermally activated and increases exponentially with temperature [6]. Therefore, a rapid dissolution of sulphide precipitates occurs in the matrix during heating. Upon cooling the sample to room temperature, growth of sulphur-rich secondary phase proceeds gradually due to fast diffusion of atoms at high

temperatures, and no detectable variation in the resistivity and Hall coefficient curves appears.

Moreover, recent atom probe analysis [7] on sodium-doped lead chalcogenides and the PbTe-PbS ternary system have shown that the solubility limit of sodium concentration in the PbS precipitates is considerably higher than in the PbTe matrix in composite samples of PbTe-PbS. Although the concentration of sodium is identical for all samples in the current study, precipitation of a sulphur-rich secondary phase may result in segregation of sodium to the precipitates. Therefore, precipitation may cause some deviation in the carrier concentration of the composite. Since the observed peak in the resistivity curve during the heating of composite samples is associated with the kinetics of dissolution for precipitation reactions; the cooling resistivity curve has been used in the current report to calculate the figure of merit.

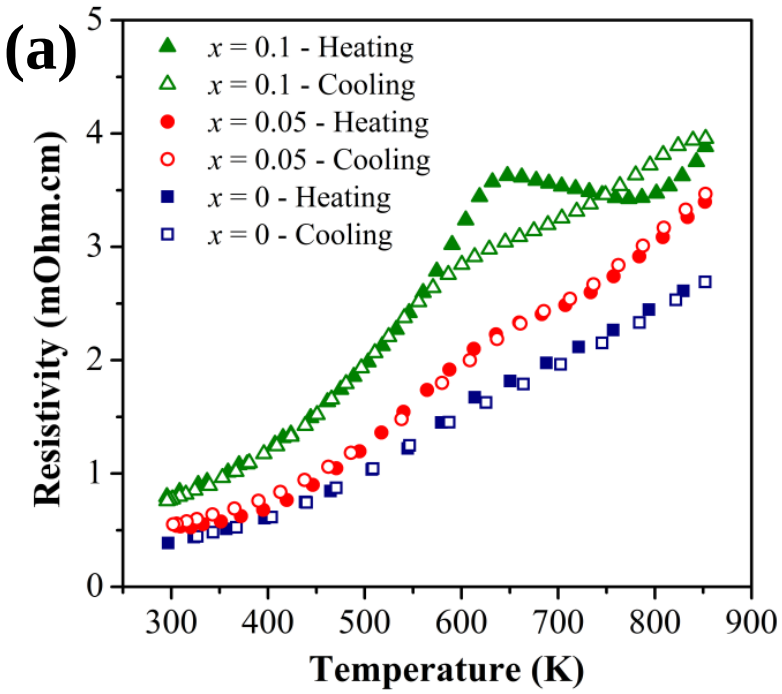

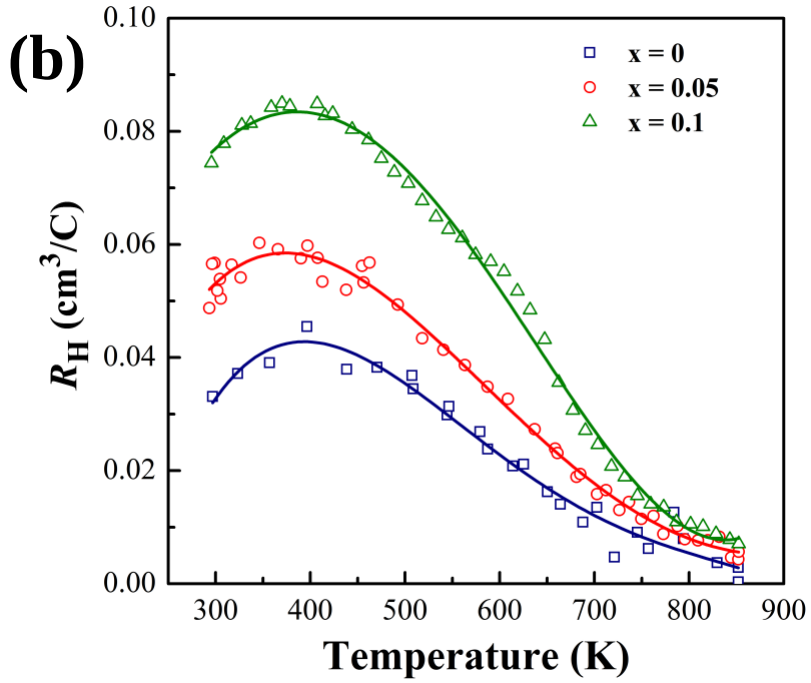

Figure S3. *Temperature-dependence of: (a) the electrical resistivity (mΩ·cm) of* $Pb_{0.98}Na_{0.02}S_xSe_{0.1}Te_{(1-x)}$ *(x = 0, 0.05 and 0.1) sintered bulk sample over a measurement cycle of heating (filled symbols) and cooling (empty symbols); indicating that the heating and cooling resistivity curves are overlapped for single phase samples (x = 0, 0.05) and demonstrate a hysteresis for the sample with x = 0.1 which shows secondary phases of sulphides; (b) Hall coefficient,* R_H, *of* $Pb_{0.98}Na_{0.02}S_xSe_{0.1}Te_{(1-x)}$ *(x = 0, 0.05 and 0.1) sintered bulk sample, showing a deviation from smoothly declining curve for the sample with x = 0.1.*

The valence band structure of lead chalcogenides (PbTe, PbSe, and PbS) can be described by a non-parabolic Kane band at the L point of the Brillouin zone (L band) and a parabolic band along the Σ line of the Brillouin zone[4] as schematically demonstrates in Figure S4. The Hall coefficient of heavily doped *p*-type PbTe remains almost constant at temperatures below 100 K and then gradually increases to reach a maximum value at around 400 K. As the temperature rises, the light valence band gradually lowers its energy and reaches the Σ-band edge. Therefore, the carriers can access the chemical potential states of both the light and the heavy valence bands [4]. This proposed two-valence-band model in PbTe and its alloys is

believed to be correlated with the observed peak in the Hall coefficient values to the temperature of valence band convergence.

The Hall coefficient is related to the carrier density (n_H), through the Hall prefactor, r_H, in the relation $n_H = r_H / eR_H$. We calculated the carrier concentration for the samples assuming that $r_H = 1$, but only for the purpose of comparison with previous studies. The results are summarised in Table S1. The concentration of sodium, dopant, is identical for all samples of the current study (1 at %) but as the fraction of PbS in the compound increases, a higher Hall coefficient is obtained over the temperature range of 300-850 K as shown in Figure S3 (b). It might be attributed to the changing energy band structure of PbTe as a result of PbS addition

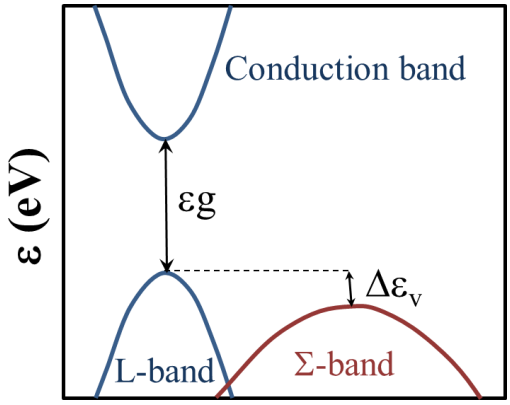

Figure S4: The relative energies of different bands of PbTe: the conduction band, the light valence band at the L point, and the heavy valence band at the ∑ line. ε_g shows the room temperature band gap, and $\Delta\varepsilon_V$ demonstrates the energy offset between the L and ∑ valence bands.

Table S1: The room temperature Hall carrier concentration for samples $Pb_{0.98}Na_{0.02}S_xSe_{0.1}Te_{(1-x)}$ (x = 0, 0.05 and 0.1).

Sample	$x = 0$	$x = 0.05$	$x = 0.1$
Hall Carrier concentration (cm^{-3}) at room temperature	1.6×10^{20}	1.1×10^{20}	8.3×10^{19}

The temperature dependant of Hall carrier mobility ($\mu_H = R_H / \rho$) in the temperature range of 300-850 K are shown in Figure S5 for samples $Pb_{0.98}Na_{0.02}S_xSe_{0.1}Te_{(1-x)}$ (x = 0, 0.05 and

0.1). The fact that the Hall carrier mobility shows insignificant variations by PbS concentration remains unexplained.

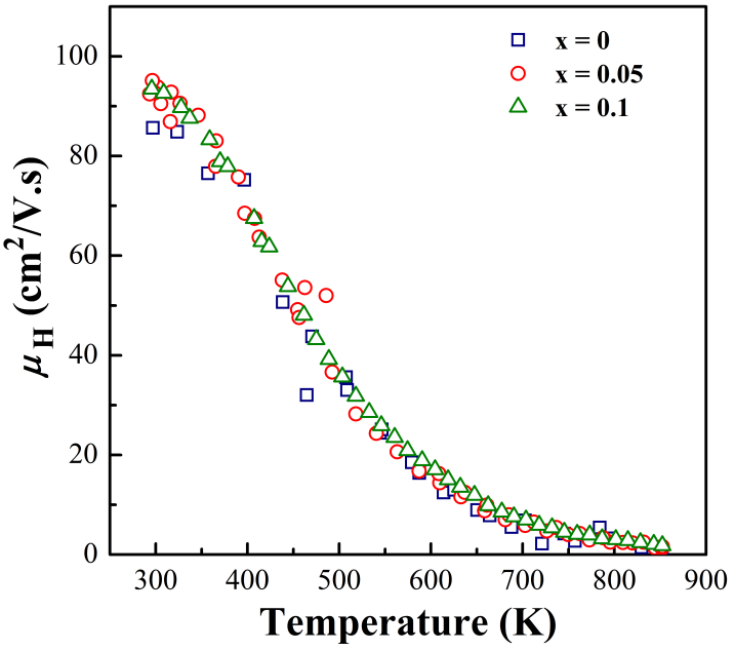

Figure S5. Temperature-dependence Hall carrier mobility (cm^2/V.s) of $Pb_{0.98}Na_{0.02}S_xSe_{0.1}Te_{(1-x)}$ (x = 0, 0.05 and 0.1) sintered bulk sample

Thermal conductivity

The thermal conductivity κ of samples are calculated from $\kappa = \rho D_T C_p$. The laser flash method (Netzsch LFA457) was used to measure thermal diffusivity D_T, density, ρ, was calculated using the measured weight and dimensions., and the specific heat capacity, Cp, was estimated by [8]:

$Cp(k_B \text{ per atom}) = 3.07 + 4.7 \times 10^{-4} \times (T/K - 300)$.

The temperature dependence of the measured thermal diffusivity, D_T, and calculated Cp are shown in Figure S6 (a) and (b) respectively.

The lattice thermal conductivity, κ_L, was obtained by subtracting the electronic component, κ_e. The value of charge carrier thermal conductivity κ_e can be determined via Widemann-

Franz relation, $\kappa_e = LT/\rho$. where ρ is the resistivity, and L is the Lorenz number estimated as a function of temperature, through fitting the reduced chemical potential η obtained from the Seebeck coefficient, S, as expressed in equation 1. The acoustic phonon scattering and single parabolic band (SPB) model [9] was assumed for this calculation.

$$S = \frac{k}{e}\left(\frac{2F_1(\eta)}{F_0(\eta)} - \eta\right) \quad (1)$$

Where the Fermi integrals F_j are:

$$F_j(\eta) = \int_0^\infty f\varepsilon^j d\varepsilon = \int_0^\infty \frac{\varepsilon^j d\varepsilon}{1+\exp(\varepsilon-\eta)} \quad (2)$$

The η values that fit the temperature dependant S is used to calculate L through equation 3:

$$L = \left(\frac{k}{e}\right)\frac{3F_0(\eta)F_2(\eta) - 4F_1(\eta)^2}{F_0(\eta)^2} \quad (3)$$

At high temperatures, where the non-parabolic heavy hole band contributes to the electronic transport properties, this relation might be interrupted slightly. This rough estimation has been shown to be reasonably consistent with a more detailed model calculation taking the band non parabolicity and multiband conduction effects into account [10]. The temperature dependence of the calculated Lorenz number is shown in Figure S7.

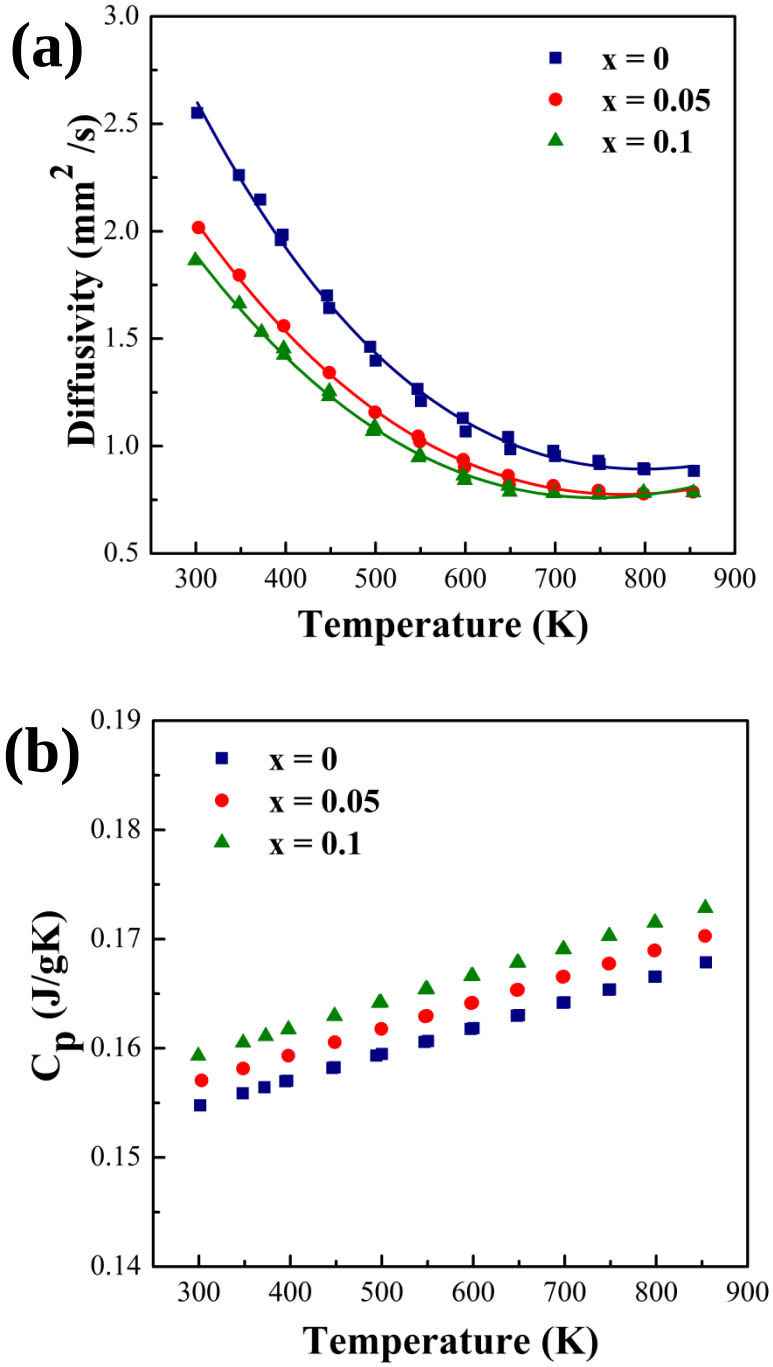

Figure S6: Temperature dependence of (a) Measured thermal diffusivity, D_T, (mm^2/s);(b) calculated Heat capacity, Cp (J/gK), of $Pb_{0.98}Na_{0.02}S_xSe_{0.1}Te_{(1-x)}$ (x = 0, 0.05 and 0.1) sintered bulk sample

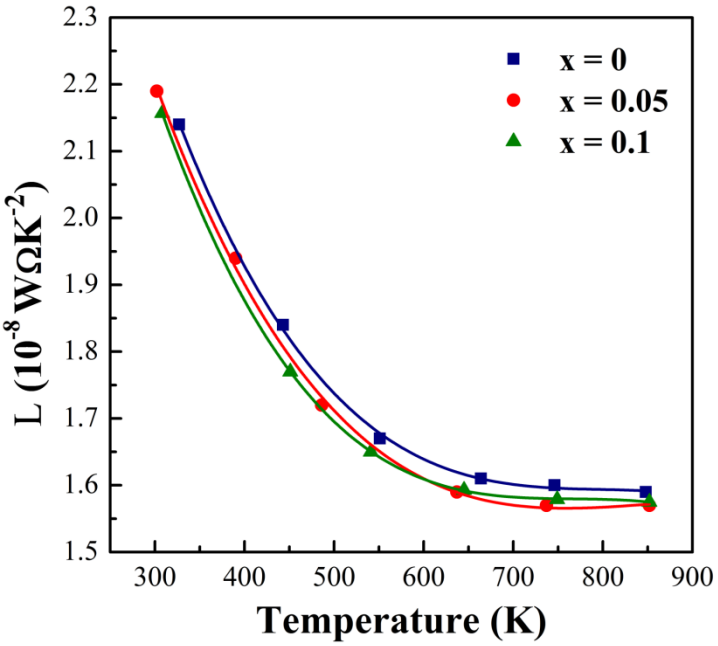

Figure S7: Temperature dependence calculated Lorenz number, L (10^{-8} $W\Omega/K^2$) of $Pb_{0.98}Na_{0.02}S_xSe_{0.1}Te_{(1-x)}$ (x = 0, 0.05 and 0.1) sintered bulk sample

References

1. **K. A. Borup, E. S. Toberer, L. D. Zoltan, G. Nakatsukasa, M. Errico, J.-P. Fleurial, B. B. Iversen and G. J. Snyder, *Rev. Sci. Instrum.*, 2012, 83, 123902-123907.**
2. **J. He, L.-D. Zhao, J.-C. Zheng, J. W. Doak, H. Wu, H.-Q. Wang, Y. Lee, C. Wolverton, M. G. Kanatzidis and V. P. Dravid, *J. Am. Chem. Soc.*, 2013, 135, 4624-4627.**
3. **S. Aminorroaya Yamini, T. Ikeda, A. Lalonde, Y. Pei, S. X. Dou and G. J. Snyder, *J. Mat. Chem. A*, 2013, 1, 8725-8730.**
4. **Y. I. Ravich, B. A. Efimova and I. A. Smirnov, *Semiconducting lead chalcogenides* Plenum Press in New York, 1970.**
5. **A. Volykhov, L. Yashina and V. Shtanov, *Inorg. Mater.*, 2006, 42, 596-604.**
6. **H. Mehrer, *Diffusion in Solids, Fundamentals, Methods, Materials, Diffusion-Controlled Processes*, Springer-Verlag Berlin Heidelberg, New York, 2007.**
7. **J. He, I. D. Blum, H.-Q. Wang, S. N. Girard, J. Doak, L.-D. Zhao, J.-C. Zheng, G. Casillas, C. Wolverton, M. Jose-Yacaman, D. N. Seidman, M. G. Kanatzidis and V. P. Dravid, *Nano Lett.*, 2012, 12, 5979-5984.**
8. **A. S. Pashinkin, M. S. Mikhailova, A. S. Malkova and V. A. Fedorov, *Inorg. Mater.*, 2009, 45, 1226-1229.**
9. **A. F. May, E. S. Toberer, A. Saramat and G. J. Snyder, *Phys. Rev. B*, 2009, 80, 125205.**
10. **Y. Pei, X. Shi, A. LaLonde, H. Wang, L. Chen and G. J. Snyder, *Nature*, 2011, 473, 66-69.**